

Curvature effects in interfacial acidity of amphiphilic vesicles

Petch Khunpetch,^{1,*} Arghya Majee,^{2,†} Hu Ruixuan,³ and Rudolf Podgornik⁴

¹*Department of Physics, Faculty of Science, Ramkhamhaeng University, Bang Kapi, Bangkok, Thailand & School of Physical Sciences, University of Chinese Academy of Sciences, Beijing, China*

²*Max Planck Institute for the Physics of Complex Systems, 01187 Dresden, Germany*

³*School of Physical Sciences, University of Chinese Academy of Sciences, Beijing, China*

⁴*School of Physical Sciences, University of Chinese Academy of Sciences, Beijing, China & Kavli Institute for Theoretical Sciences, University of Chinese Academy of Sciences, Beijing, China & CAS Key Laboratory of Soft Matter Physics, Institute of Physics, Chinese Academy of Sciences, Beijing,*

China & Wenzhou Institute of the University of Chinese Academy of Sciences, Wenzhou, Zhejiang, China

(Dated: May 18, 2023)

We analyze the changes in the vicinal acidity (pH) at a spherical amphiphilic membrane. The membrane is assumed to contain solvent accessible, embedded, dissociable, charge regulated moieties. Basing our approach on the linear Debye-Hückel as well as the non-linear Poisson-Boltzmann theory, together with the general Frumkin-Fowler-Guggenheim adsorption isotherm model of the charge regulation process, we analyse and review the dependence of the local pH on the position, as well as bulk electrolyte concentration, bulk pH and curvature of the amphiphilic single membrane vesicle. With appropriately chosen adsorption parameters of the charge regulation model, we find a good agreement with available experimental data.

I. INTRODUCTION

The charging state of phospholipid membranes [1], lipid nanoparticles [2], but also other amphiphilic [3] as well as proteinaceous self-assemblies [4], is governed by the protonation/deprotonation equilibria of dissociable surface molecular groups in contact with the aqueous subphase. In the case of proteins [5] the negative charges stem from the deprotonated carboxylate on the side chains of aspartic and glutamic acid, and the deprotonated hydroxyl of the phenyl group of tyrosine, while the positive charge originates from the protonated amine group of arginine and lysine, as well as the protonated secondary amine of histidine [6]. In the case of phospholipids the negative charge is derived from deprotonated phosphate groups and deprotonated carboxylate, while the positive charge, though rare in naturally occurring lipids [7], stems from protonated amine group or other titratable molecular moieties with an engineered dissociation constant [8].

Among the phenomena in biomolecular assemblies where charging equilibria are particularly important, one can specifically name the electrostatic interactions between membranes [9], ion transport across the membranes [10], as well as the insertion and translocation of membrane proteins [11]. To these well known examples one could also add the emerging role of charging equilibria in viral proteinaceous capsid shells [12], their interactions with various substrates [13] and structural reconstructions and maturation processes in chimeric protein-lipid capsid shells [14–16].

The charging equilibria in biomacromolecular assemblies typically involve local pH and local bathing solution ion concentrations, which - as has been recognized for a while - in general differ from the bulk conditions [6, 17, 18], implying that the changes in the bathing solution properties will affect not only the pH sensing and pH response of lipid membranes [19] but will also - and even more importantly - affect the membrane protein(s) entering different biochemical reactions required for the sustainability and proliferation of life. Elucidating the quantitative details of the relation between *bulk* and *local* solution properties thus constitutes one of the challenges in the description of biomacromolecular assemblies.

We have recently formulated [20–22] a theoretical model that couples the full macroscopic continuum description of electrostatic interactions with the surface protonation/deprotonation reactions of charged lipids and/or other amphiphilic molecules [8]. This model not only yields the details of the lipid charging state as a function of the curvature and bathing solution parameters, such as pH and salt concentration but also, and this will be the focus here, the full spatial profile of the pH in the vicinity of the membrane. In this way we can connect the interfacial curvature with the interfacial pH for the non-planar self-assemblies and assess the role of the surface curvature in the interfacial acidity/basicity properties. This connection in itself attests to the fact that the knowledge of the *bulk* bathing solution properties does not imply that we know what the *local* solution properties are, that in the last instance determine the solution state near the proteins and lipids functional groups. Below we will argue that the local pH can actually veer off quite far from the nominal values set in the bulk.

In what follows we will first recapitulate the basic fea-

* petch.k@rmail.ru.ac.th; Co-first and co-corresponding author

† majee@pks.mpg.de; Co-first and co-corresponding author

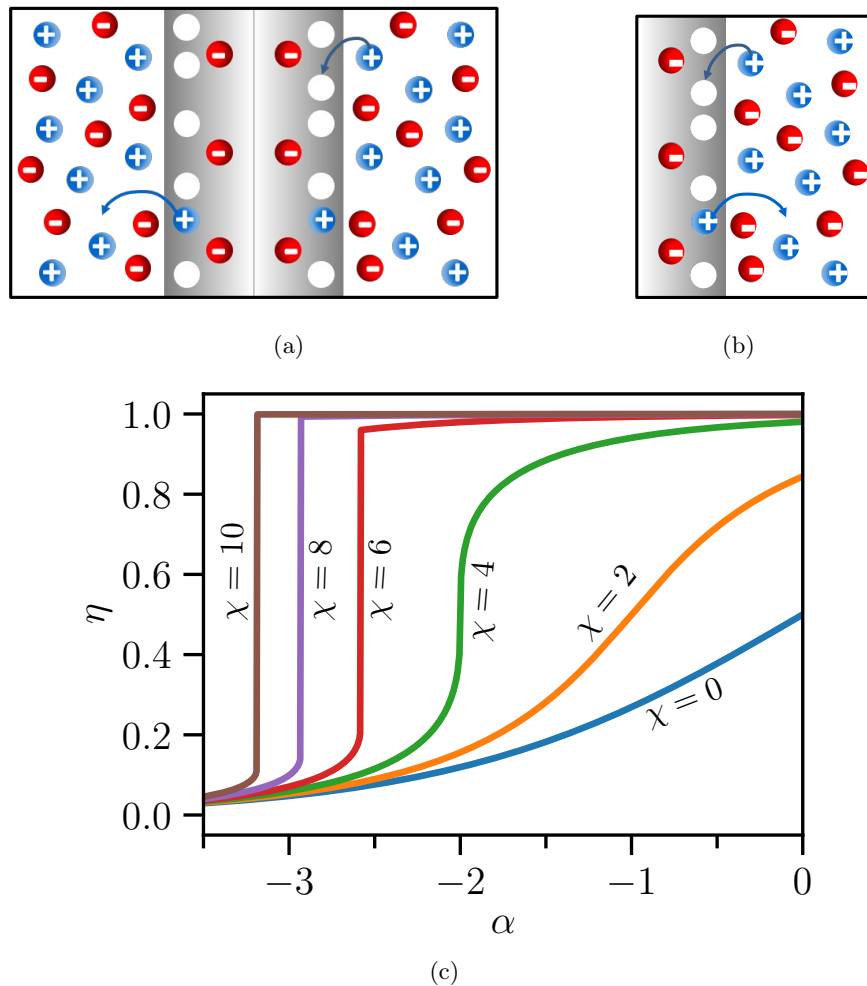


FIG. 1. (a) A schematic representation of charge regulation at the surface of an amphiphilic bilayer containing dissociable protonation/deprotonation sites. In model (1), Eq. (1), the charge is regulated in the interval $-\sigma_0 \leq \sigma_{1,2} \leq \sigma_0$. In the case of the model (2) Eq. (2) the charge is regulated in the interval $0 \leq \sigma_{1,2} \leq \sigma_0$. In both cases σ_0 is a fixed maximal structural charge density. Protons provided by the dissociable surface moieties can exchange with the solution and in the process charge/discharge the dissociable groups. (a) Charge regulated bilayer membrane with CR sites on the surfaces of both monolayers. (b) A single monolayer of the charge regulating bilayer. (c) Solution of the Frumkin-Fowler-Guggenheim isotherm, Eq. (12), for a single charge regulated monolayer with different values of the χ interaction parameter with $\psi = 0$. The critical isotherm is given by $\chi = -2\alpha$, corresponding to $(\alpha, \chi) = (-2, 4)$, and below this value there is a discontinuous, first order transition from one charged state to another one. $\chi = 0$ corresponds to the Langmuir isotherm with no discontinuous charging state transition.

tures of our theoretical model with the Poisson-Boltzmann volume free energy functional for mobile charges and the Frumkin-Fowler-Guggenheim adsorption isotherm model, formulated in terms of the appropriate surface free energy, for the surface charging equilibrium. We then solve the model in the linearized Debye-Hückel (DH) approximation as well as in the full Poisson-Boltzmann (PB) theory for a spherical vesicle with finite thickness permeable membrane, whose solvent accessible surfaces contains the dissociable moieties. We specifically describe the spatial profiles of the vicinal as well as luminal pH as a function of the parameters of the model. We finally comment on the salient features of the interfacial acidity and its dependence on the bulk properties.

II. CHARGE REGULATION MODEL

We consider a spherical vesicle with salt solution on the two sides of its bilayer membrane, composed of two charge-regulated monolayers containing dissociable moieties, as shown in Fig. 1. The inner radius of the vesicle shell is R with charge density σ_1 and the outer radius is $R + w$ with charge density σ_2 . The approach described below broadly follows our previous work and we shall only list the relevant details that were further elaborated in [8, 20–22]. We will focus on two CR models corresponding either to a symmetric charge regulation, with the surface charge density $-\sigma_0 \leq \sigma_{1,2} \leq \sigma_0$, or an asymmetric CR models with the surface charge density $0 \leq \sigma_{1,2} \leq \sigma_0$, where

$\sigma_0 = e_0 n_0$ is a structural charge parameter corresponding to the maximal dissociated surface charge, with e_0 the elementary charge ($e_0 > 0$) and n_0 a structural density of dissociable moieties.

Furthermore, we assume that $\eta_{1,2} \in [0, 1]$ are the fractions of the neutral lipid heads where the adsorption/desorption (association/dissociation) of as yet unspecified cations can take place on the inner and outer monolayers and that $\sigma_{1,2}$ and $\eta_{1,2}$ are uniform over the two monolayers.

In model (1) [20] the CR surface charge density is then given by

$$\sigma_i = 2n_i e_0 \left(\eta_i - \frac{1}{2} \right), \quad (1)$$

with $-e_0 n_{1,2} \leq \sigma_{1,2} \leq e_0 n_{1,2}$ that can obviously change sign, while in model (2) [23] we assume that the CR surface charge density is given by

$$\sigma_i = n_i e_0 (\eta_i - 1), \quad (2)$$

so that $-e_0 n_{1,2} \leq \sigma_{1,2} \leq 0$ and consequently cannot change sign. We note that the two models described by Eq. (1) and Eq. (2) correspond to two situations, where the protonation/deprotonation of dissociable moieties can lead to positive or negative net charge, or it leads only to a single type of net charge. In the first case the model is charge-symmetric while in the second case it is charge-asymmetric. In reality the situation is probably somewhere in between with an additional compositional asymmetry associated with the outer and inner monolayer.

In numerical calculations the static dielectric constant of water is assumed as $\epsilon_w = 80$ and that of the lipid bilayer membrane as $\epsilon_p = 5$. The Debye screening length ($\lambda_D = \kappa_D^{-1}$) varies from about 0.34 nm to 10.75 nm, corresponding to the monovalent salt concentration ranging from 1 – 0.001M [24]. Moreover, we define $\mu = \epsilon_p / \epsilon_w$.

III. ELECTROSTATIC FREE ENERGY: POISSON-BOLTZMANN AND DEBYE-HÜCKEL FORMS

We start with the standard PB free energy, or the DH free energy in the linearized case, that depends on the distribution of mobile charges, assumed to belong to a univalent electrolyte with a fixed bulk chemical potential. The surface charges are assumed to be located at both interfaces of a spherical membrane. Most of our results pertain to the DH approximation that has proven to be useful not only to provide qualitative but also quantitative results in the context of various problems involving interactions of charged colloidal particles [20, 21, 25–28]. We should, however, clearly state that the linearization implied by the DH approximation pertains only to electrostatics but not to the surface charging equilibrium which is always considered in its full, non-linear form.

There are various ways to write down the PB free energy [29] and we choose the field description, with the radially varying mean-field electrostatic potential $\psi(r)$ as the only relevant variable. The total PB electrostatic free energy is then given by

$$\mathcal{F}_{ES} = - \int_V dV \left[\frac{\epsilon_w \epsilon_0}{2} \left(\frac{d\psi(r)}{dr} \right)^2 + 2n_I (\cosh \beta e_0 \psi(r) - 1) \right] + \oint_{A_1} dA_1 \psi(R_1) \sigma_1 + \oint_{A_2} dA_2 \psi(R_2) \sigma_2, \quad (3)$$

where n_I is the univalent electrolyte concentration in the bulk, $R_1 = R$ and $R_2 = R + w$, while the equilibrium value of $\psi(r)$ is obtained from the corresponding Euler-Lagrange (EL) equation. The volume integral extends over all the regions except the bilayer interior. Within the bilayer interior there are no mobile charges and the second term in the square brackets is absent so that the electrostatic free energy is simply

$$\mathcal{F}_{ES} = - \frac{\epsilon_p \epsilon_0}{2} \int_V dV \left(\frac{d\psi(r)}{dr} \right)^2 + \oint_{A_1} dA_1 \psi(R_1) \sigma_1 + \oint_{A_2} dA_2 \psi(R_2) \sigma_2, \quad (4)$$

where the volume integral now extends over the bilayer interior and of course, the permittivity ϵ_p needs to be used.

A common approach to electrostatic effects in soft matter and specifically in the case of charged membrane vesicles is *via* the DH approximation [30] often coupled together with small curvature, second order expansion [7, 31, 32]. In the DH approximation, valid strictly for $\beta e_0 \psi(r) \ll 1$ but yielding qualitatively similar results to the full PB solution also outside this limit [8], the corresponding expressions for the electrostatic free energy Eq. (3) simplifies considerably to

$$\mathcal{F}_{ES} = - \frac{\epsilon_w \epsilon_0}{2} \int_V dV \left(\left(\frac{d\psi(r)}{dr} \right)^2 + \kappa_D^2 \psi(r)^2 \right) + \oint_{A_1} dA_1 \psi(R_1) \sigma_1 + \oint_{A_2} dA_2 \psi(R_2) \sigma_2, \quad (5)$$

where the inverse square of the Debye screening length λ_D is given by $\kappa_D^2 = 2n_I \beta e_0^2 / (\epsilon_w \epsilon_0)$ and the volume integral again extends over all the regions except the bilayer interior. While the free energies Eq. (3) and Eq. (5) imply the PB and the DH equation in the regions accessible to electrolyte ions [25], respectively, Eq. (4) leads to the standard Laplace equation inside the lipid dielectric core. Inserting the solution of the EL equations back into Eq. (5), it is then further reduced to a form corresponding

to the Casimir charging process [33]

$$\begin{aligned} \mathcal{F}_{ES}(\sigma_1, \sigma_2, R) &= 4\pi \sum_{i=1}^2 R_i^2 \int_0^{\sigma_i} d\sigma_i \psi(\sigma_1, \sigma_2, R_i) \\ &\rightarrow \frac{1}{2} \sum_{i=1}^2 4\pi R_i^2 \sigma_i \psi(\sigma_1, \sigma_2, R_i), \quad (6) \end{aligned}$$

where the right arrow indicates the DH limit of the same expression where the potentials are linear functions of the charge density. With the explicit solution for the electrostatic potential, see Appendix IX A, we can derive the DH expression for the electrostatic free energy per area as a function of the radius of curvature R to inverse quadratic order [24], obtaining an approximate but highly accurate form of the free energy

$$\begin{aligned} \frac{\kappa_D \epsilon_0 \epsilon_w \mathcal{F}_{el}(\sigma_1, \sigma_2, R)}{2\pi R^2} &= f_0(\sigma_1, \sigma_2, \kappa_D, w) \\ &+ \frac{f_1(\sigma_1, \sigma_2, \kappa_D, w)}{\kappa_D R} \\ &+ \frac{f_2(\sigma_1, \sigma_2, \kappa_D, w)}{(\kappa_D R)^2}, \quad (7) \end{aligned}$$

where the curvature independent terms, $f_0(\sigma_1, \sigma_2, \kappa_D, w)$, $f_1(\sigma_1, \sigma_2, \kappa_D, w)$ and $f_2(\sigma_1, \sigma_2, \kappa_D, w)$ are explicitly given in the Appendix IX C. In general the above free energy density of a curved membrane is not symmetric in the two solvent accessible surface charge densities that were assumed to be constant.

The DH electrostatic free energy for fixed surface charges displays a general quadratic dependence on the curvature of the lipid bilayer. This quadratic dependence of electrostatic free energy was standardly taken as a point of departure for the electrostatic renormalization of the mechanical properties of membranes, such as surface tension and bending rigidity [24, 34–38] but ceases to be the case of charge regulated membranes.

IV. CHARGE REGULATION FREE ENERGY AND SELF-CONSISTENT BOUNDARY CONDITIONS

Assuming that the inner and outer membrane surfaces are chemically identical we presume that the surface charge regulation process can be described by the Frumkin-Fowler-Guggenheim adsorption isotherm, which is a two parameter adsorption model [39], parameterized with the adsorption energy, α , the interaction energy between adsorbed ions, χ , and the lattice gas entropy. For $\chi = 0$ the Frumkin-Fowler-Guggenheim model reduces to the Langmuir model. Other, multiparametric models of variable complexity can be defined but will not be analyzed here [40].

The corresponding charge regulation free energy densities of the inner and outer membrane surfaces denoted

by $i = 1, 2$ are given by

$$\begin{aligned} \frac{\mathcal{F}_{CR}(\eta_i)}{4\pi R_i^2} &= n_0 k_B T \left[-\alpha \eta_i - \frac{\chi}{2} \eta_i^2 \right. \\ &\left. + \eta_i \ln \eta_i + (1 - \eta_i) \ln(1 - \eta_i) \right]. \quad (8) \end{aligned}$$

This can be furthermore normalized w.r.t. the inner area $4\pi R^2$ which is used later. The first two terms in the free energy are enthalpic in origin. The other terms are the lattice gas mixing entropy of charged sites with the surface area fraction η and neutralized sites with the surface area fraction $1 - \eta$.

In the case of phospholipids such as Phosphatidic acid (PA, smallest and simplest phospholipid, precursor for other phospholipids), Phosphatidylserine (PS) and Phosphatidylglycerol (DPPG), the negative charge comes from deprotonated conjugate base of phosphoric acid and deprotonated carboxylate, while the positive charge comes from the protonated amine or ammonium head of cationic lipids but can be also substituted with an engineered dissociation constant.

In these cases of charge regulation the adsorb-ing/desorbing particles are identified as protons and α is then the deprotonation free energy difference [41] which in the case of the Langmuir adsorption model [23] becomes

$$\alpha = (\text{p}K_a - \text{pH}) \ln 10, \quad (9)$$

where $\text{p}K_a$ is the dissociation constant of the deprotonation reaction and $\text{pH} = -\log_{10}[\text{H}^+]$ is the acidity. The Langmuir model in this context is equivalent to a Henderson-Hasselbalch equation with electrostatics included [42]. Furthermore, χ , as in the related lattice regular solutions theories (e.g., the Flory-Huggins theory [43]) describes the short-range interactions between nearest neighbor (de)protonation sites [44]. A parameter value $\alpha \leq 0$ encodes a favorable adsorption free energy, while $\chi \geq 0$ represents the tendency of particles on the macroion surface adsorption sites to phase separate into domains. Fig. 1 displays a schematic depiction of the charge regulation process and the Frumkin-Fowler-Guggenheim adsorption isotherm as a function of α for different values of the interaction parameter χ .

It is important to reiterate at this point that other charge regulation models are of course possible and have been proposed for various dissociable groups in different contexts [39, 40, 45]. Our reasoning in choosing the particular Frumkin-Fowler-Guggenheim isotherm was guided by its simplicity in the way it takes into account the salient features of the dissociation process on the membrane surface, and the fact that the implied phenomenology has been analyzed before in the context of charged amphiphilic systems [46].

From the general electrostatic free energy Eq. 6 we then obtain the surface electrostatic potential as

$$\frac{\partial \mathcal{F}_{ES}(\sigma_1, \sigma_2, R)}{\partial \sigma_i} = 4\pi R_i^2 \psi(\sigma_1, \sigma_2, R_i), \quad (10)$$

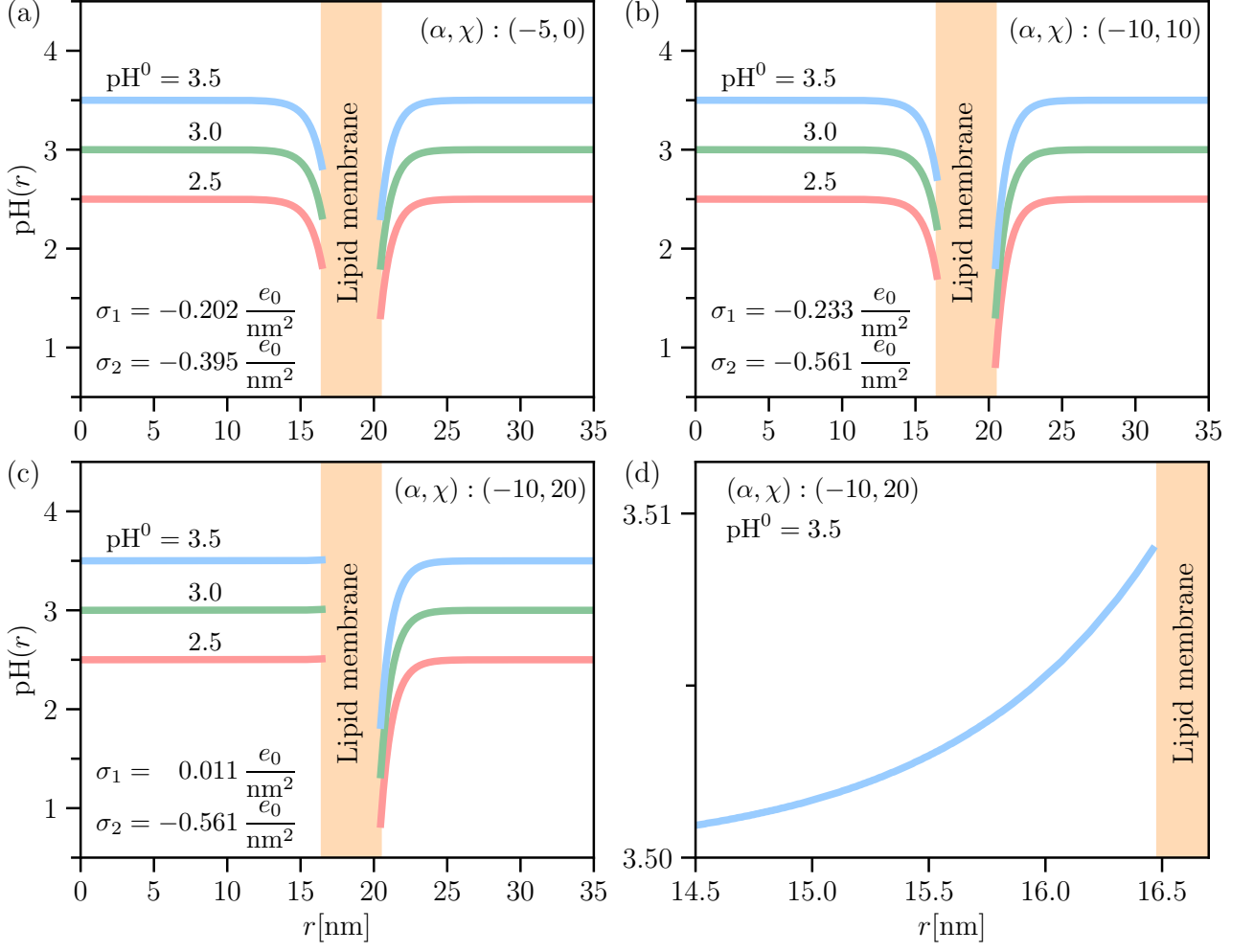


FIG. 2. Plot of $\text{pH}(r)$ across the membrane for different values of bulk pH^0 and $(\alpha, \chi) = (-5, 0)$ [panel (a)], $(\alpha, \chi) = (-10, 10)$ [panel (b)]. In both cases $\kappa_D = 1.215 \text{ nm}^{-1}$ and $R = 16.46 \text{ nm}$ with dimensionless curvature h fixed at 0.05. The Bjerrum length $\ell_B = 0.74 \text{ nm}$, $\epsilon_p = 5$, $\epsilon_w = 80$, surface dissociable group concentration $n_0 = 1 \text{ nm}^{-2}$, and $w = 4 \text{ nm}$. σ_1 and σ_2 are obtained from the CR process. All curves show that the pH vicinal to the bilayer reduces remarkably from pH^0 in the bulk. pH at the outer surface is lower than that right at the inner surface and then increases exponentially towards pH^0 in the region far from the outer surface. (c)-(d) left panel $(\alpha, \chi) = (-10, 20)$, right panel magnification for pH close to the inner surface. All curves show that, pH does not change much from pH^0 . However, at the region close to the inner surface, we can observe change in pH that grows as $\sinh(\kappa_D r)$. Again, the pH goes exponentially towards pH^0 in the outer region.

for $i = 1, 2$. By considering Eqs. (10), as well as the form of the charge regulation free energy Eq. (8) we derive the standard Frumkin-Fowler-Guggenheim adsorption isotherm [39, 45] from the thermodynamic equilibrium obtained by minimizing the total free energy of the system. We get two equations that correspond to charge regulation boundary conditions

$$\frac{\partial \mathcal{F}_{ES}(\sigma_1, \sigma_2, R)}{\partial \sigma_i} + \frac{\partial \mathcal{F}_{CR}(\eta_i)}{\partial \eta_i} = 0 \quad (11)$$

for $i = 1, 2$, which by taking into account Eq. (10) can be solved by an implicit equation for $\eta_i = \eta_i(\psi)$ [20, 21, 44, 47] in the form

$$\eta_i(\psi) = \left(1 + e^{-\alpha - \chi \eta_i(\psi) + 2\beta e_0 \psi}\right)^{-1} \quad (12)$$

with $\eta_i(\psi) = \eta_i(\psi(\sigma_1, \sigma_2, R_i))$. The numerical solution of the above equation is presented in Fig. 1 and corresponds to the Frumkin-Fowler-Guggenheim adsorption isotherm. Again we reiterate that the DH linearization pertains only to electrostatics, first term in Eq. 11, while the surface charging equilibrium, is always considered in its full, non-linear form. It is evident from Fig. 1 that for $\chi \leq -2\alpha$ the adsorption isotherm exhibits a discontinuous transition, whereas above the “critical isotherm”, $\chi = -2\alpha$, i.e., $\chi \geq -2\alpha$, it remain continuous.

The boundary condition derived above, Eq. 11, together with the solution of either full PB equation or the linearized DH version for the electrostatic free energy Eq. (7) constitute the basic equations of our model. In the case of the linear theory with the electrostatic free

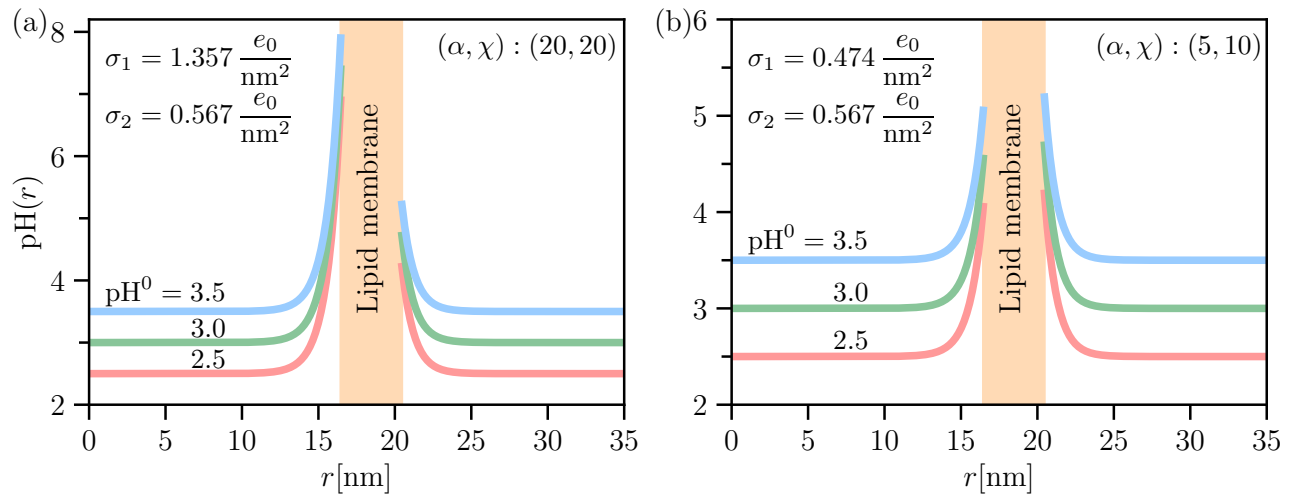


FIG. 3. Plot of $\text{pH}(r)$ across the membrane. We have chosen $(\alpha, \chi) = (20, 20)$ (a) and $(\alpha, \chi) = (5, 10)$ (b), $\kappa_D = 1.215 \text{ nm}^{-1}$ and $h = (\kappa_D R)^{-1} = 0.05$. All curves show that, at the region close to the inner surface of the vesicle, pH increases as $\sinh(\kappa_D r)$. The pH decreases exponentially towards pH^0 in the region far from the outer surface for both panels (a) and (b). The Bjerrum length $\ell_B = 0.74 \text{ nm}$, $\epsilon_p = 5$, $\epsilon_w = 80$, surface dissociable group concentration $n_0 = 1 \text{ nm}^{-2}$, and $w = 4 \text{ nm}$.

TABLE I. pH at the inner and outer surfaces of the vesicle. The bulk pH^0 is set as 5.2. The radius of the vesicle is 100 nm. The Bjerrum length $\ell_B = 0.74 \text{ nm}$, $\epsilon_p = 5$, $\epsilon_w = 80$, surface dissociable group concentration $n_0 = 1 \text{ nm}^{-2}$, and $w = 4 \text{ nm}$. The inverse Debye length is $\kappa_D = 0.5 \text{ nm}^{-1}$.

(α, χ)	$\sigma_1(e_0/\text{nm}^2)$	$\sigma_2(e_0/\text{nm}^2)$	$\text{pH}(r = R)$	$\text{pH}(r = R + w)$
(10, 0)	0.232	0.280	7.003	7.268
(10, 20)	0.587	0.777	9.767	10.930
(20, 20)	0.876	0.921	11.961	12.035
(20, 10)	0.646	0.797	10.218	11.091
(-5, 10)	0	0	5.2	5.2
(-10, 20)	0	0	5.2	5.2
(-10, 10)	-0.130	-0.165	4.190	3.979
(-20, 5)	-0.429	-0.526	1.871	1.310

energy given by Eq. (7) we obtain the surface potentials from Eq. (10) as $\psi(R_i) = \psi_i(\eta_1, \eta_2)$.

Finally we should note that our approach is based on the free energy of the CR process and not on the assumed isotherms that would follow from some chemical equilibrium considerations as is often done in the literature. While the two approaches are in principle equivalent, it seems to us that the free energy approach has a more universal appeal and allows also the explicit calculation of the total free energy, i.e., ES plus CR.

V. COMPARISON BETWEEN THE FULL PB AND THE APPROXIMATE DH SOLUTIONS

The DH approximation [30] is standardly invoked in order to derive limiting expressions and analytical formu-

lae in various contexts of macromolecular electrostatics [27, 28]. In order to be able to substantiate our usage of the DH approximation for most of the numerical results, we compare the pH profile resulting from the full PB equation with the consequences of the linearized DH equation. Again, we point out that the linearization applies only to the electrostatic part, but not to the charge regulation part. Sometimes the linearization is extended also to that case of charge regulation [48] as in the constant regulation boundary condition often invoked by Borkovec *et al.* [49], where for large separations one may expand the charge-potential relationships at the surface around the potential at infinite separation.

We compare quantitatively the PB and the DH results for certain choices of the model parameters in Appendix IX B. The general conclusion is that qualitatively, and often also quantitatively, they generally coincide but ex-

TABLE II. pH at the inner and outer surfaces of the vesicle. The bulk pH^0 is set as 5.2. The radius of the vesicle is 100 nm. The Bjerrum length $\ell_B = 0.74$ nm, $\epsilon_p = 5$, $\epsilon_w = 80$, surface dissociable group concentration $n_0 = 1 \text{ nm}^{-2}$, and $w = 4$ nm. The inverse Debye length is $\kappa_D = 1.0 \text{ nm}^{-1}$.

(α, χ)	$\sigma_1(e_0/\text{nm}^2)$	$\sigma_2(e_0/\text{nm}^2)$	$\text{pH}(r = R)$	$\text{pH}(r = R + w)$
(5, 5)	0.376	0.452	6.641	6.889
(10, 0)	0.449	0.515	6.918	7.128
(10, 20)	1.078	0.922	9.307	8.662
(20, 10)	1.078	0.922	9.307	8.662
(-5, 10)	0	0	5.2	5.2
(-10, 20)	0	0	5.2	5.2
(-10, 10)	-0.284	-0.362	4.111	3.846
(-15, 10)	-0.563	-0.697	3.040	2.595

hibit differences in certain parts of the parameter space. It seems that one can thus safely use the DH approximation if the focus is on the qualitative features, whereas a PB based calculation would be needed in order to do quantitative comparisons.

VI. INTERFACIAL AND LUMINAL PH

The above derivation and specifically the definition $\alpha = (\text{p}K_a - \text{pH}) \ln 10$ assume that the concentration of the protons in solution is much lower than the concentration of salt and does not contribute to the spatial profile of the electrostatic potential, neither on the PB nor the DH level. For many dissociable moieties at physiological solution conditions this assumption holds well, but in general a more detailed implementation of the pH effects is needed, see e.g., [50, 51].

With the above provisos the local pH is a “passive” variable in the solution, except at the surface of the lipid bilayer where it determines the dissociation state. The spatial dependence of $\text{pH} = -\log_{10} [\text{H}^+]$ is obtained from the electrostatic potential as

$$\begin{aligned} \text{pH}(r) &= -\log_{10} [\text{H}^+](r) \\ &= -\log_{10} [\text{H}^+]_0 + \beta e_0 \psi(r) \log_{10} e \\ &= \text{pH}^0 + \beta e_0 \psi(r) \log_{10} e, \end{aligned} \quad (13)$$

where $\text{pH}^0 = -\log_{10} [\text{H}^+]_0$ is either the pH in the outside bulk reservoir, or the inside pH that is set by the procedure of vesicle preparation and can coincide or can be different from the bulk value [52]. The calculation of $\text{pH}(r)$ then follows from the electrostatic potential profile that is written explicitly in the DH approximation in Appendix IX A, yielding the pH profile in the interior of the vesicle as

$$\text{pH}(r \leq R) = -\log_{10} [\text{H}^+]_0 + \beta e_0 \log_{10} e A \frac{\sinh(\kappa_D r)}{r}, \quad (14)$$

where κ_D is the inverse Debye length and A is given in the Appendix IX A. Outside the vesicle the relevant dependence is obtained as

$$\text{pH}(r \geq R) = -\log_{10} [\text{H}^+]_0 + \beta e_0 \log_{10} e B \frac{\exp(-\kappa_D r)}{r} \quad (15)$$

with B given in the Appendix IX A. Obviously both inside as well as outside the vesicle the local pH decays with the Debye length. The two constants $A = A(\sigma_1, \sigma_2, \kappa_D w, \kappa_D R)$ and $B(\sigma_1, \sigma_2, \kappa_D w, \kappa_D R)$ are linear functions of the internal and external surface membrane charge densities. The above formulae allow us to explicitly obtain the spatial variation of pH around and across the membrane as well as the drops in pH either across the membrane, or between the bulk reservoir and the region adjacent to the membrane.

Note that while the electrostatic potential is well defined also inside the membrane, the pH is not since the protons do not move freely across the hydrophobic kernel of the membrane.

Because the pH exhibits a spatially varying profile, $\text{pH} = \text{pH}(r)$, we can define different characteristic values that can be, at least in some cases, obtained either directly or indirectly from experiments [11, 53]. First we can define a drop in pH across the membrane of the vesicle of magnitude

$$\Delta \text{pH}_m = \text{pH}(R + w) - \text{pH}(R). \quad (16)$$

Two other important quantifiers are the difference between the bulk pH^0 and pH right at the outer surface as a function of the outer radius of the vesicle R , defined as

$$\Delta \text{pH}_{\text{out}} = \text{pH}(R + w) - \text{pH}^0. \quad (17)$$

Similarly, the difference between the bulk value pH^0 and pH right at the inner surface as a function of the inner radius of the vesicle R , defined as

$$\Delta \text{pH}_{\text{in}} = \text{pH}(R) - \text{pH}^0. \quad (18)$$

In what follows we will present several notable numeric results while at the same time reminding the reader that this is a multi-parameter system and its parameter space cannot be explored exhaustively and systematically at this point.

A separate question here is the value of the potential, or equivalently the pH, at the center of the vesicle relevant

$$\lim_{r \rightarrow 0} \psi(r) = \psi(0) = \frac{\epsilon_w \sigma_1 R^2 \kappa_D w^2 + \epsilon_p [\sigma_1 R^2 + \sigma_2 (R+w)^2] R + \epsilon_w \sigma_1 (1 + \kappa_D R) w R^2}{\epsilon_0 \epsilon_w \{(\epsilon_p - \epsilon_w) w^2 + \epsilon_p R^2\}} \operatorname{csch}(\kappa_D R), \quad (19)$$

taking into account the Appendix IX A. The pH in the lumen then follows as

$$\text{pH}(0) = -\log_{10} [\text{H}^+]_0 + \beta e_0 \log_{10} e \psi(0), \quad (20)$$

where $\log_{10} [\text{H}^+]_0$ is the acidity in the bulk reservoir. The expression for $\text{pH}(0)$ has two well defined limits defined by

$$\lim_{\kappa_D R \ll 1} \psi(0) = \frac{\epsilon_p [\sigma_1 R^2 + \sigma_2 (R+w)^2] + \epsilon_w \sigma_1 w R}{\epsilon_0 \epsilon_w \{(\epsilon_p - \epsilon_w) \kappa_D w^2 + \epsilon_p \kappa_D R^2\}}, \quad (21)$$

and

$$\lim_{\kappa_D R \gg 1} \psi(0) = \frac{\epsilon_w \sigma_1 R (R+w) 2(\kappa_D R) (\kappa_D w) e^{-\kappa_D R}}{\epsilon_0 \epsilon_w \{(\epsilon_p - \epsilon_w) \kappa_D w^2 + \epsilon_p \kappa_D R^2\}}. \quad (22)$$

Clearly in the second limit of $\kappa_D R \gg 1$ the potential in the center of the vesicle vanishes and thus the luminal pH is the same as in the bulk, if the membrane is fully permeable to all mobile charged species. Interestingly enough, as can be discerned from numerical solution, the electrostatic potential and consequently the pH inside the vesicle are almost constant up to the inner surface, implying that the Donnan potential approximation could be used for that case [54]. These are the only analytical limits that one can derive for this problem.

Finally, we note that our calculation is based on the chemical equilibrium and ionic identity between the ionic solution inside and outside the vesicle.

VII. RESULTS

We now analyze some numerical results obtained mostly within our model (1) unless specifically annotated for model (2).

We first investigate the full spatial profile of pH in the vicinity of the vesicle. We assume that in the preparation of the vesicle the inner and the outer solution are equilibrated at the same bathing solution pH. On the DH level the solution for the potential can be derived analytically, see Appendix IX A, but the solution of the

for the analysis of the lumina of viruses and virus-like particles [54]. Here again, we invoke the differences stemming from the different procedures of preparation that can constrain the value of the inner pH to be different from the bulk, a situation we will not analyze in detail. In the case of the DH, small curvature approximation this is found to be

CR isotherm, Eq. (11), can only be obtained numerically. The latter then yields the two surface charge densities, $\sigma_{1,2}$. Figures 2-3 show the plots of pH vs r obtained from Eq. (13) for different values of the bulk pH^0 and the CR parameters α, χ . Clearly the general dependence of $\text{pH}(r)$ indicates a large variation close to both surfaces of the bilayer, to be quantified below.

We have used typical system parameters such as an inverse Debye length $\kappa_D = 1.215 \text{ nm}^{-1}$, or equivalently, screening length $\lambda_D = 0.823 \text{ nm}$ corresponding to an aqueous electrolyte solution with 140 mM salt concentration. The dimensionless curvature h is defined as $h = 1/(\kappa_D R)$, where R is the inner radius of the vesicle. In Figs. 2 and 3, the dimensionless curvature h is fixed at 0.05 corresponding to $R = 16.46 \text{ nm}$.

From our Frumkin-Fowler-Guggenheim charge regulation model, we obtain ($\sigma_1 = -0.202 e_0/\text{nm}^2, \sigma_2 = -0.395 e_0/\text{nm}^2$) for ($\alpha = -5, \chi = 0$) (no surface interaction) (Fig. 2(a)) and ($\sigma_1 = -0.233 e_0/\text{nm}^2, \sigma_2 = -0.561 e_0/\text{nm}^2$) for ($\alpha = -10, \chi = 10$) (Fig. 2(b)). The plots show that pH decreases remarkably at the region close to the vesicle's inner surface and that the pH at the outer surface is lower than that at the inner surface. In general the pH approaches exponentially the bulk pH^0 away from the membrane. For negative $\alpha = -10$ and $\chi = 20$ ($\chi = -2\alpha$) case, (Fig. 2(c)), the Frumkin-Fowler-Guggenheim charge regulation model yields ($\sigma_1 = 0.011 e_0/\text{nm}^2, \sigma_2 = -0.561 e_0/\text{nm}^2$). Close to the surface the pH increases like $\sinh(\kappa_D r)$ which is shown with more detail in Fig. 2(d).

For positive $\alpha > 0$, Fig. 3, we obtain ($\sigma_1 = 1.357 e_0/\text{nm}^2, \sigma_2 = 0.567 e_0/\text{nm}^2$) at ($\alpha = 20, \chi = 20$) (Fig. 3(a)) and ($\sigma_1 = 0.474 e_0/\text{nm}^2, \sigma_2 = 0.567 e_0/\text{nm}^2$) at ($\alpha = 5, \chi = 10$) (Fig. 3(b)). All curves exhibit the same scaling $\sinh(\kappa_D r)$ near the inner surface. Clearly in the case of $\alpha > 0$ the local pH decreases from the value it attains near the surface of the bilayer towards the bulk pH^0 for both Figs. 3(a) and 3(b).

In order to see the deviation of pH from the bulk pH^0 clearly, we have used $\kappa_D = 1/20 \text{ nm}^{-1}$ and $R = 10 \text{ nm}$ with dimensionless curvature h fixed at 2. Figure 4 presents the plot of $\text{pH}(r)$ across the membrane for bulk

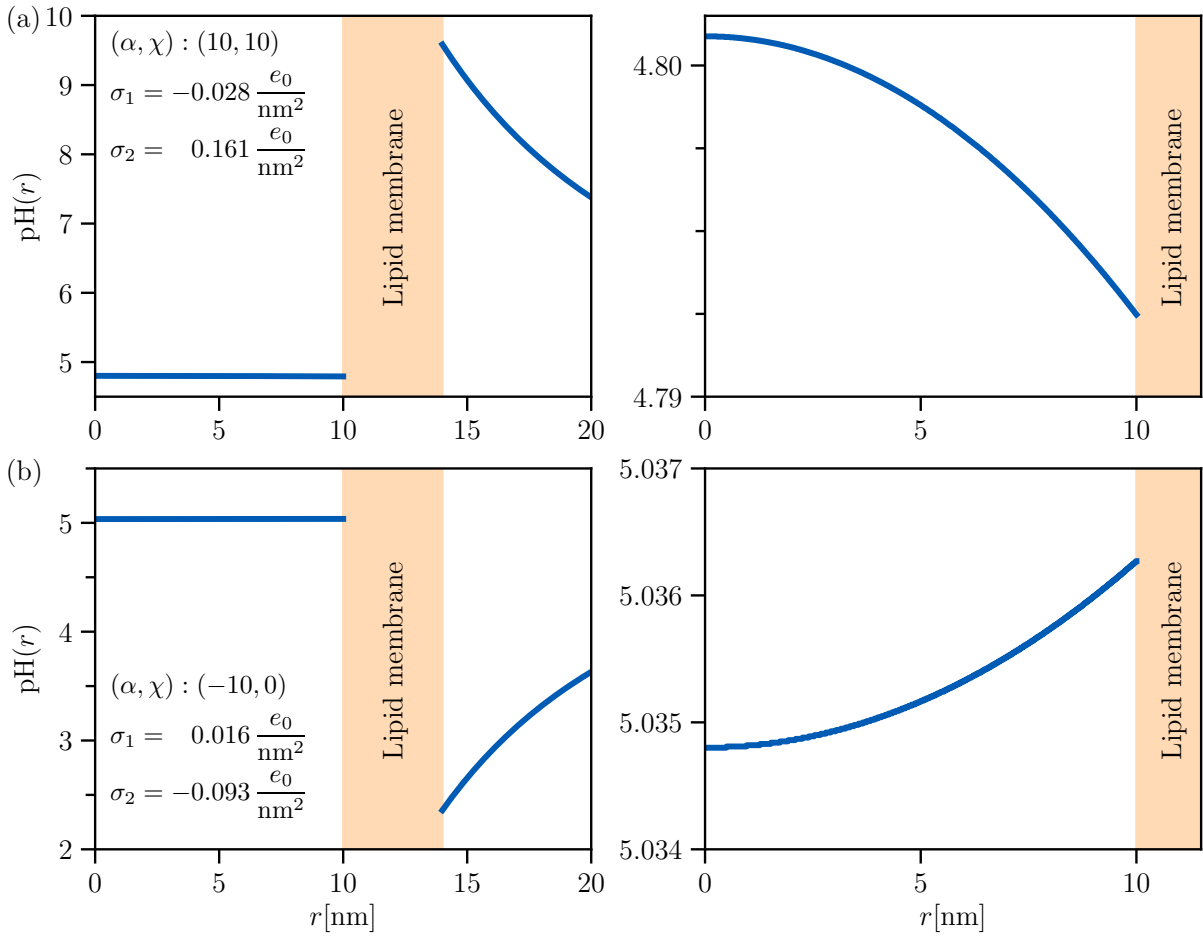


FIG. 4. Plot of $\text{pH}(r)$ across the membrane for bulk $\text{pH}^0 = 5.0$, panel (a) $(\alpha, \chi) = (10, 10)$, panel (b) $(\alpha, \chi) = (-10, 0)$. The right most panels show the expanded $\text{pH}(r)$ scale in order to see the small changes with r . In both cases $\kappa_D = 1/20 \text{ nm}^{-1}$ and $R = 10 \text{ nm}$ with dimensionless curvature h fixed at 2. σ_1 and σ_2 are obtained from the CR process and correspond to the values of (α, χ) combination. The vicinal pH close to the outer surface of the vesicle can be drastically different from the bulk one, depending on the parameters. The Bjerrum length $\ell_B = 0.74 \text{ nm}$, $\epsilon_p = 5$, $\epsilon_w = 80$, surface dissociable group concentration $n_0 = 1 \text{ nm}^{-2}$, and $w = 4 \text{ nm}$.

$\text{pH}^0 = 5.0$, $(\alpha, \chi) = (10, 10)$ (Fig. 4(a)), $(\alpha, \chi) = (-10, 0)$ (Fig. 4(b)). The right most panels show the expanded $\text{pH}(r)$ scale in order to see the small changes with r . The vicinal pH close to the outer surface of the vesicle can be drastically different from the bulk one, depending on the parameters.

We now analyze the dependence of the $\Delta\text{pH}_{\text{out}}$ on the various parameters of the system in Figs. 5 and 6. The procedure is again the same as before, we solve analytically for the electrostatic potential and then obtain the corresponding surface charges from the Frumkin-Fowler-Guggenheim charge regulation model. The inverse Debye length is set as $\kappa_D = 1.215 \text{ nm}^{-1}$. Of particular importance is the dependence on the curvature of the bilayer. In Figs. 5 and 6 we show this dependence for positive and negative α . Clearly at first $\Delta\text{pH}_{\text{out}}$ starts with a positive value, meaning that the surface pH is larger than the bulk pH^0 . It then increases with curvature, reaches a maximum and then decays, eventually even turning negative. This

behavior is the more pronounced the more α is negative. For positive values of α , $\Delta\text{pH}_{\text{out}}$ starts with a negative value, reaches a minimum and then increases, eventually turning positive. Interestingly enough, because of the properties of the Frumkin-Fowler-Guggenheim isotherm, for small curvatures $\Delta\text{pH}_{\text{out}}$ can start at zero, see Fig. 6(a), for certain negative values of α . This simply means that at that α, h the bilayer is uncharged, charges up at a critical value of curvature and then follows basically the same behavior as for other negative values of α . The pronounced variation of $\Delta\text{pH}_{\text{out}}$, which is in principle measurable [11], indicates that one could get some indication for the numerical values of the model parameters by comparing with suitable experiments.

In a recent detailed experimental work on detection of curvature-dependent interfacial pH for amphiphilic self-assemblies and unilamellar phospholipid vesicles an interface-interacting spiro-rhodamine pH probe and Schiff base polarity probe have been used to measure the de-

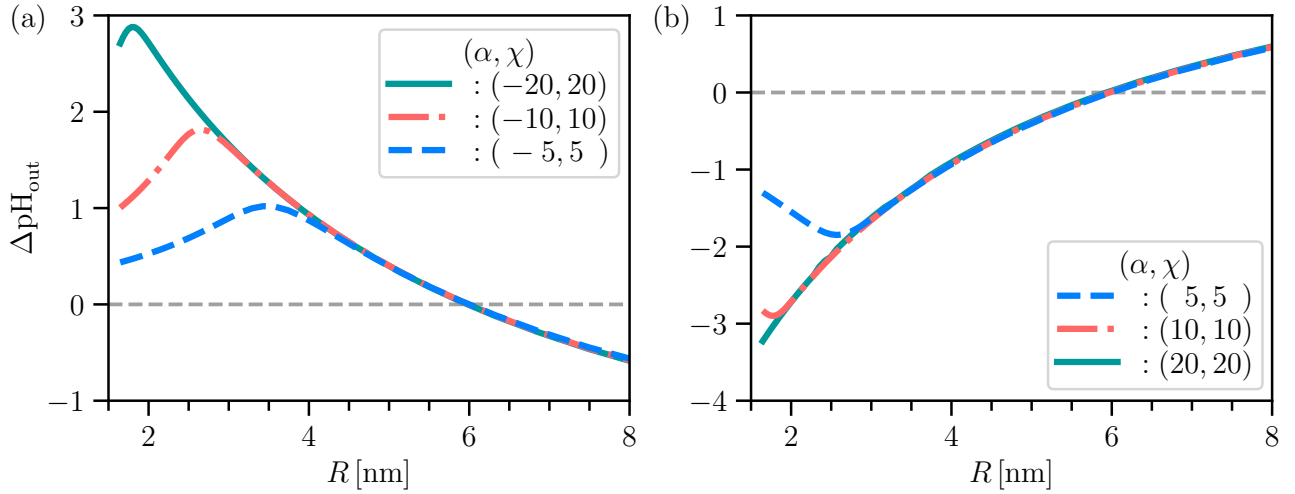


FIG. 5. Plot of $\Delta\text{pH}_{\text{out}}$ as defined in Eq. (17) vs R with $\kappa_D = 1.215 \text{ nm}^{-1}$. Clearly the pH vicinal but exterior to the vesicle can be larger or smaller than the bulk pH^0 , depending on the charge regulation parameters entering into the CR model. In general, $\alpha \leq 0$ makes the vicinal pH larger, while $\alpha \geq 0$ makes it smaller. Also, the larger χ the larger is this effect.

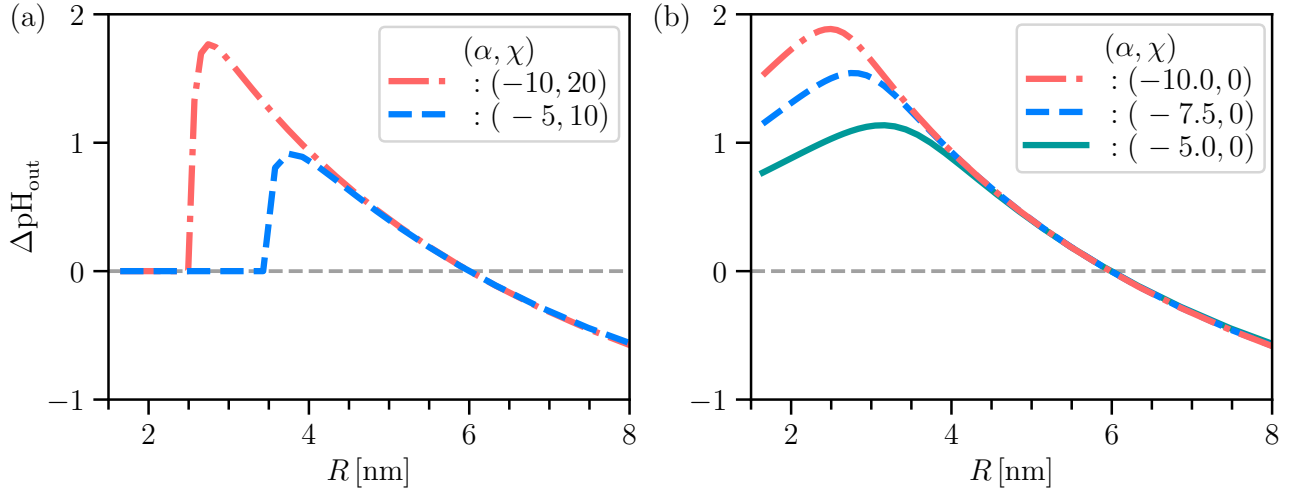


FIG. 6. Plot of $\Delta\text{pH}_{\text{out}}$ vs R for different values of (α, χ) and $\kappa_D = 1.215 \text{ nm}^{-1}$. (a) $\chi = -2\alpha$. (b) $\alpha < 0$ and $\chi = 0$ (no surface interaction). For large enough positive χ the dependence of $\Delta\text{pH}_{\text{out}}$ on R shows a behavior akin to a second order transition, where for small radii it vanishes, and then at a critical value $R = R_c$ it starts deviating from zero, reaching for a maximum and then levelling off at a constant value for a sufficiently large R . No such behavior is observed for $\chi = 0$.

viation of the local interfacial pH from the bulk phase [11]. It has been shown that the charging state (and polarity) of the amphiphile and phospholipid self-assemblies can be regulated by the curvature of the vesicle/micelle. While the experimental system is more complicated than our model and specifically contains also the interfacial dielectric constant we believe it could be instructive to compare the predictions of our model with the measured values for $\Delta\text{pH}_{\text{out}}$.

We calculated $\text{pH}(r = R)$ and $\text{pH}(r = R + w)$ from the Frumkin-Fowler-Guggenheim CR model as described in detail above. The curvature radius R is set as 100 nm which is one of the experimentally chosen values for the large unilamellar phospholipid vesicles in the experiment

[11]. Other examples include radii $\sim 15, 25, 50$ nm that we did not consider explicitly. We assumed the bulk value $\text{pH}^0 = 5.2$ corresponding to the 2.0 mM cacodylate-HCl buffer. The inverse ionic screening length was taken as $\kappa_D = 0.5 \text{ nm}^{-1}$ (Table 1.) and $\kappa_D = 1.0 \text{ nm}^{-1}$ (Table 2.), corresponding to ionic concentrations of 25 mM and 100 mM. For both choices $\text{pH}(r = R)$ and $\text{pH}(r = R + w)$ are larger than the bulk pH^0 for $\alpha > 0$ and less than the bulk pH^0 for $\alpha < 0$. In addition for the critical adsorption isotherm $\chi = -2\alpha$ we have $\text{pH}(r = R) = \text{pH}(r = R + w) = \text{pH}^0$ for small radii of curvature.

In experiments of [11] performed for 1,2-dimyristoyl-sn-glycero-3-phosphorylglycerol (DMPG)/1,2-dimyristoyl-sn-glycero-3-phosphocholine (DMPC) (2 : 1) mixture in the

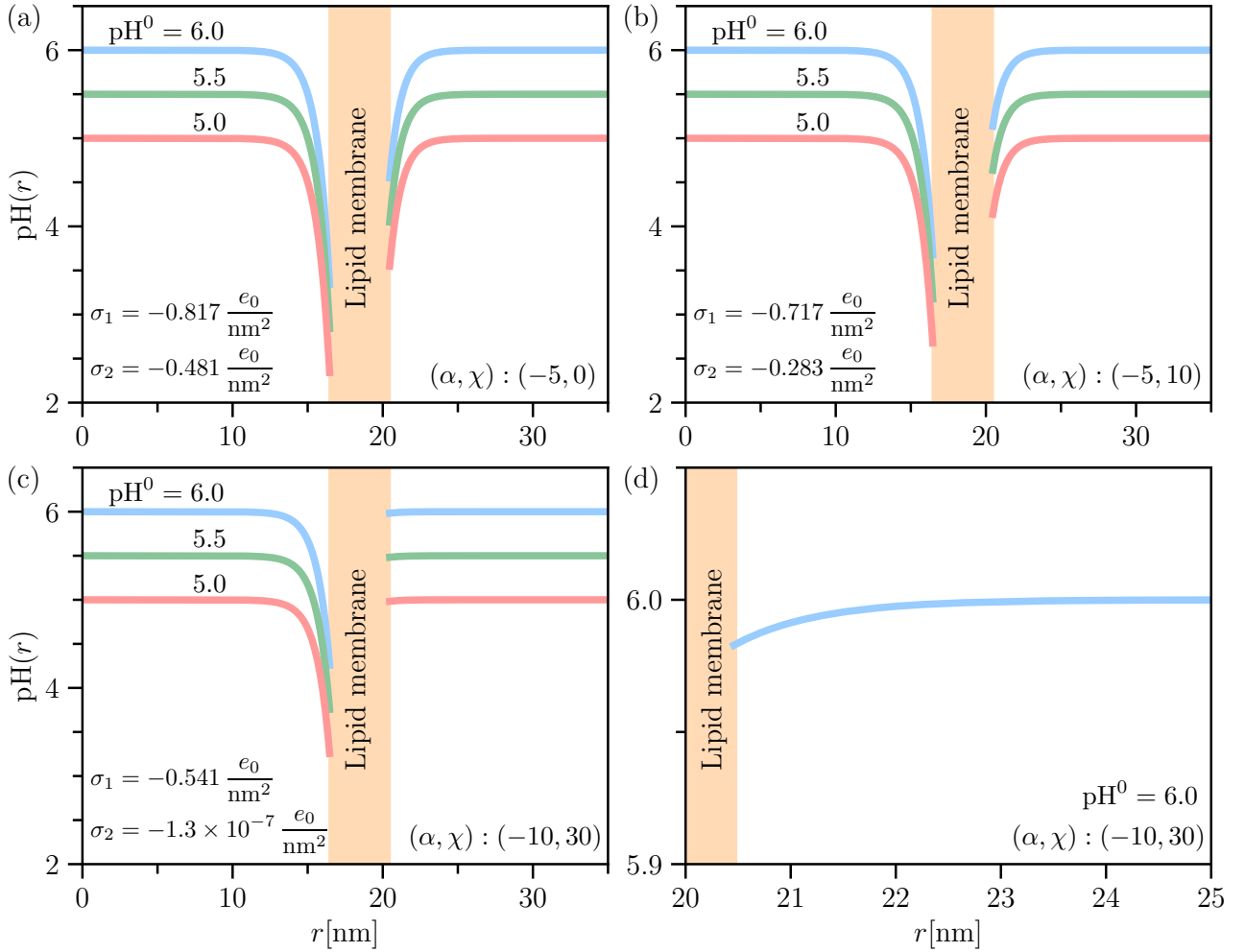


FIG. 7. Plot of $\text{pH}(r)$ across the membrane for model (2), Eq. (2), with $\kappa_D = 1.215 \text{ nm}^{-1}$ and $R = 16.46 \text{ nm}$ with dimensionless curvature h set at 0.05. The surface charge densities on both sides of the bilayer σ_1 and σ_2 are negative. For $(\alpha, \chi) = (-5, 0)$ or $(\alpha, \chi) = (-5, 10)$ the corresponding $\Delta\text{pH}_{\text{out}}$ is comparable. For $(\alpha, \chi) = (-10, 30)$, $\Delta\text{pH}_{\text{out}}$ is much smaller and the deviation of pH from pH^0 at the outer surface can only be seen clearly after magnification close to the outer surface (d).

case of large unilamellar vesicles, the authors obtained $\Delta\text{pH}_{\text{out}} \simeq -1.4$ – -1.6 . In this particular case the negative charge stems from the deprotonation of DMPG while the DMPC lipid component carries no net charge. We model this situation both in the framework of model (1), as well as model (2), which seems to be the more realistic case. From our calculations in the framework of the model (1), with $(\alpha, \chi) = (-10, 10)$, we obtain $\Delta\text{pH}_{\text{out}}$ (defined in Eq. (17)) as -1.221 (Table 1.) and -1.354 (Table 2.). Theoretically, depending on the combination of (α, χ) , the value of $\Delta\text{pH}_{\text{out}}$ from our model 1 could be obtained in the range of the experiments.

On the other hand the model (2), Fig. 7, yielding only negative values of the surface charge density and thus, as already stated, being closer to the experimental situation corresponding to DMPG deprotonation, with $(\alpha, \chi) = (-5, 0)$ and $(\alpha, \chi) = (-5, 10)$, yields $\Delta\text{pH}_{\text{out}}$ up to -1.5 , which is again close to the stated experimental value [11]. Note also that in model (2) the corresponding

CR parameters (α, χ) corresponding to a close match with experimental data are much smaller and thus possibly more realistic.

VIII. DISCUSSION

The properties of the bulk bathing solution can be quite different from the local environment near the embedded membrane proteins and lipid functional groups. This is in particular important for the spatial dependence of the acidity/basicity that actually governs the dissociation equilibrium of protein and lipid dissociable groups. Recent detailed experiments [11, 53] have in fact shown that the surface pH can differ from the bulk one by several units. A deviation of 1.8 and 2.2 units from the bulk to the interface was detected for cationic cetrimonium bromide (CTAB) micelles and dimethyldioctadecylammonium bromide (DDAB) unilamellar vesicles [53], and the

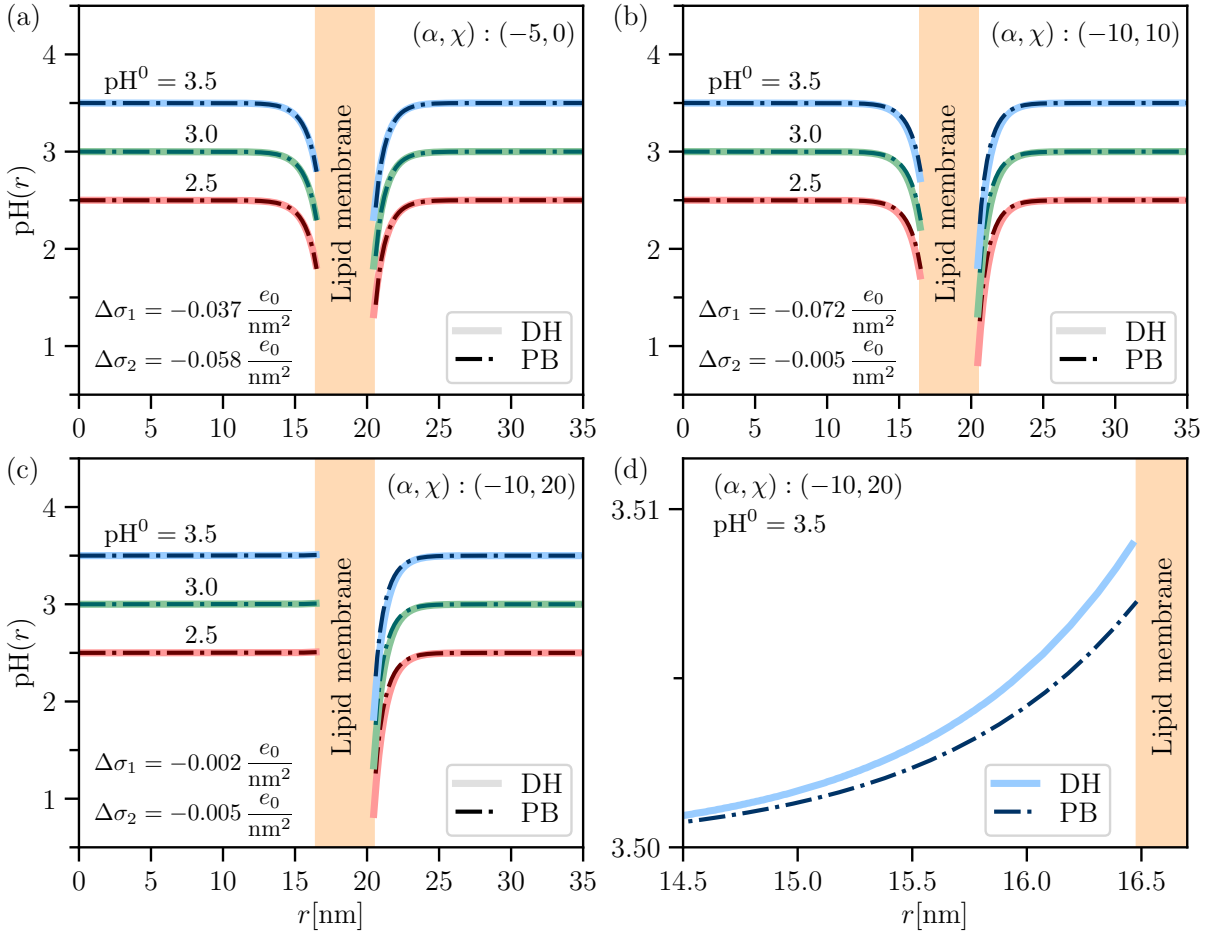


FIG. 8. Comparison of the spatial dependence of $\text{pH}(r)$ across the membrane for different values of the bulk pH^0 obtained from the full PB and the linearized DH solutions in the case of $\alpha \leq 0$. (a) $(\alpha, \chi) = (-5, 0)$, (b) $(\alpha, \chi) = (-10, 10)$, (c) $(\alpha, \chi) = (-10, 20)$ for different values of the bulk pH^0 and (d) an expanded view of the region vicinal to the membrane for $\text{pH}^0 = 3.5$. Here $\Delta\sigma_i = \sigma_i^{\text{PB}} - \sigma_i^{\text{DH}}$. The absolute value of σ_i is greater within the full PB theory, but it changes when there is a symmetry breaking, i.e., for $(\alpha, \chi) = (-10, 20)$. $\Delta\sigma_1$ is negative here but σ_1 is positive in this case, implying that $\sigma_1^{\text{PB}} < \sigma_1^{\text{DH}}$. The largest discrepancies are observed in the vicinity of the membrane but even then they are overall small.

pH deviation of -1.4 to -1.6 for DMPG/DMPC (2 : 1) mixture large unilamellar vesicles [11], respectively.

Motivated by these experimental findings we performed a detailed theoretical study of the effects of interfacial curvature in the case of a bilayer vesicles with surface dissociable groups, on the interfacial acidity/basicity properties and found that the local pH can actually veer off quite far from the nominal values set in the bulk. Our theoretical model is based on the Poisson-Boltzmann volume free energy functional for mobile charges and the Frumkin-Fowler-Guggenheim adsorption isotherm model, formulated in terms of the appropriate surface free energy, for the surface dissociation equilibrium. It quantifies the surface adsorption/dissociation energy, the nearest neighbor surface interaction energy and the lattice gas entropy of adsorption/dissociation sites. In general the model is rich enough to encode the simple Langmuir isotherm behavior captured also by the original charge regulation model [23] as well as the more nuanced behavior of the

Frumkin-Fowler-Guggenheim isotherm [20] and the ensuing first order adsorption/dissociation transition, see Fig. 1. We solved the model numerically on the full non-linear PB level as well as in the linearized DH approximation for a spherical vesicle with finite thickness permeable membrane, whose solvent accessible surfaces contains the dissociable moieties. We were specifically interested to derive the spatial profiles of the vicinal as well as luminal pH as a function of the parameters of the model.

The numerical solutions of our model predict the full spatial dependence of pH as a function of surface dissociation model parameters, α and χ , assumed to be the same for the outer (solution interface) as well as inner (luminal interface) bilayer surface. What is clear is that for $\alpha \leq 0$ the pH vicinal to the bilayer differs remarkably from pH^0 of the bulk, with pH at the outer surface being lower than that right at the inner surface, see Fig. 2. This behavior can be modified by the amount of salt in the bulk reservoir, or equivalently its screening length κ_D^{-1} ,

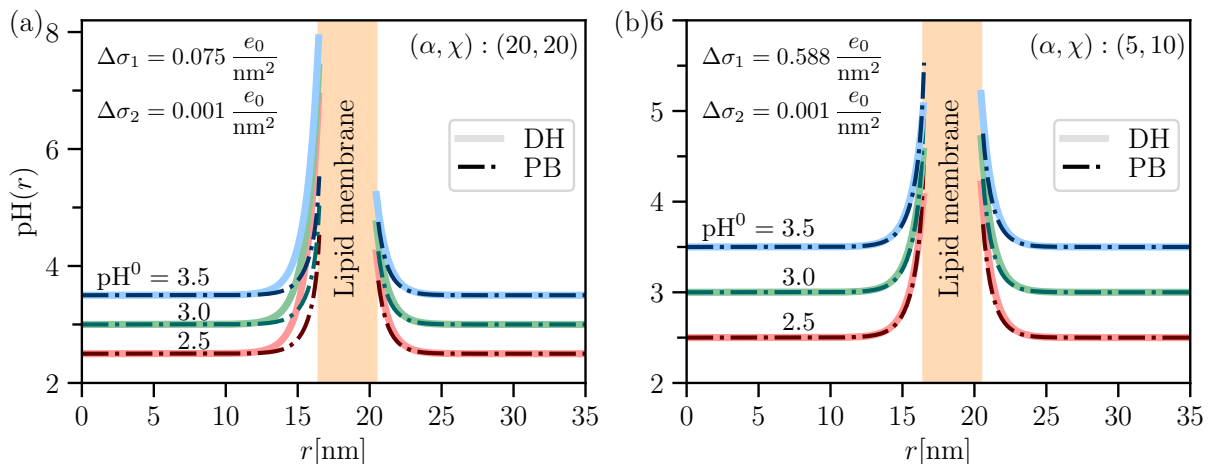


FIG. 9. Comparison of the spatial dependence of $\text{pH}(r)$ across the membrane for different values of the bulk pH^0 obtained from the full PB and the linearized DH solutions in the case of $\alpha \geq 0$. (a) $(\alpha, \chi) = (20, 20)$ and (b) $(\alpha, \chi) = (5, 10)$. One observes a significant deviation between pH values obtained from PB and DH approaches for $(\alpha, \chi) = (20, 20)$. For $(\alpha, \chi) = (5, 10)$ the difference is nevertheless small though $\Delta\sigma_1$ is higher in this case. This is because of the value of σ_1 itself which is high for $(\alpha, \chi) = (20, 20)$.

which can be seen by comparing the behavior of Figs. 2 and 4. As for the case of $\alpha \geq 0$, see Fig. 3, clearly the pH at the luminal interface is much more perturbed than at the solution interface, implying that the negative curvature has quantitatively a larger effect than the positive curvature of the interface.

We also compared two different models of CR process, one associated with a symmetric charge distribution across the bilayer (model 1), and another one with an asymmetric distribution (model 2). We note that the pH profiles obtained can be similar, the CR parameters (α, χ) corresponding to that profile are quite different, compare Figs. 2 and 7.

The change in pH at the solution interface can be quantified further by computing $\Delta\text{pH}_{\text{out}}$ as defined in Eq. (17). From Fig. 5 we discern that for $\alpha \leq 0$, $\Delta\text{pH}_{\text{out}}$ as a function of the membrane curvature develops a local maximum whose position depends on the radius of the vesicle, R , contrary to the case of $\alpha \geq 0$ where $\Delta\text{pH}_{\text{out}}$ develops a local minimum as a function of the radius of the vesicle. In both cases the position of the extremum depends also on the value of the interaction parameter χ displacing it towards the interface for larger positive values. The value of $\Delta\text{pH}_{\text{out}}$ can be either positive or negative depending on the surface interaction parameters. For some combinations of (α, χ) , $\Delta\text{pH}_{\text{out}}$ can show a second order transition as a function of R , being zero for small enough R and then starting to deviate from zero at a critical value of the radius of the vesicle, see Fig. 6. This can only happen for large enough nearest neighbor interactions at the surface, $\chi \neq 0$.

Another notable conclusion, following from the comparison between the DH approximation and the full PB solution, is that the former describes the same effects as the latter on a qualitative level. Notably, the DH approx-

imation as used here does not imply just a DH solution for the electrostatic potential but also a full minimization of the final free energy with non-linear surface interaction terms included. It would be probably more appropriate to refer to it as the DH-CR solution than as merely a DH solution. We surmise that it could be used to great advantage also in other situations where the full PB solution is prohibitively difficult to find even numerically.

FUNDING

PK, RH and RP acknowledge funding from the Key Project No. 12034019 of the National Natural Science Foundation of China and the 1000-Talents Program of the Chinese Foreign Experts Bureau.

ACKNOWLEDGEMENTS

RP, PK and HR acknowledge the support of the School of Physics, University of Chinese Academy of Sciences, Beijing. RP also acknowledges the support of the Wenzhou Institute of the University of Chinese Academy of Sciences, Wenzhou, Zhejiang.

IX. APPENDIX

A. Debye-Hückel solution

In the DH approximation, the electrostatic potential can be obtained explicitly for different regions of the

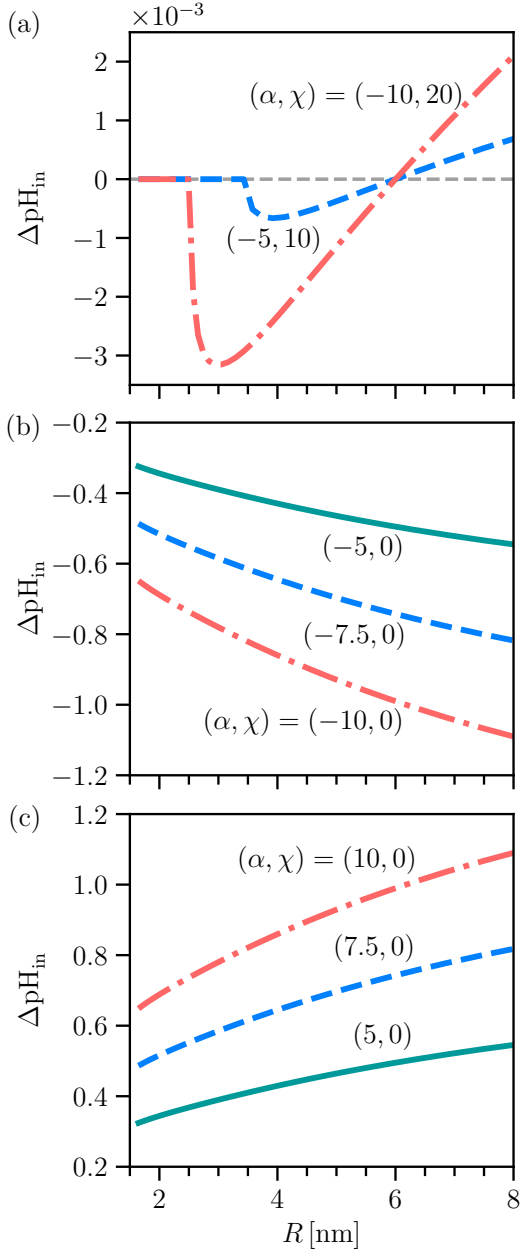


FIG. 10. Plot of $\Delta\text{pH}_{\text{in}}$ vs R for the "critical isotherm" $\chi = -2\alpha$ case (a) and for $\chi = 0$ for negative (b) and positive (c) values of α . Overall $\Delta\text{pH}_{\text{in}}$ is very small with different behaviors in a curve i.e., (i) $\Delta\text{pH}_{\text{in}} < 0$ (ii) $\Delta\text{pH}_{\text{in}} = 0$, and (iii) $\Delta\text{pH}_{\text{in}} > 0$, i.e. $\Delta\text{pH}_{\text{in}}$ can increase, decrease or remain constant as the radius R varies. (b,c) Plots of $\Delta\text{pH}_{\text{in}}$ vs R for $\chi = 0$ case, that corresponds to no surface interaction. Plots are for $\alpha < 0$ (b) and $\alpha > 0$ (c). The $\Delta\text{pH}_{\text{in}}$ in both cases are in fact the same in absolute value but different in sign. For all cases $\kappa_D = 1.215 \text{ nm}^{-1}$.

problem [55]. Inside the vesicle,

$$\frac{1}{r} \frac{d^2(r\Phi_{\text{I}}(r))}{dr^2} + \kappa_D^2 \Phi_{\text{I}}(r) = 0 \quad (23)$$

giving

$$\Phi_{\text{I}}(r \leq R) = A \frac{\sinh(\kappa_D r)}{r}. \quad (24)$$

In the lipid membrane or the amphiphilic layer we have

$$\frac{1}{r} \frac{d^2(r\Phi_{\text{II}}(r))}{dr^2} = 0 \quad (25)$$

implying

$$\Phi_{\text{II}}(R \leq r \leq R + w) = \frac{C}{r} + D, \quad (26)$$

while in the external compartment

$$\frac{1}{r} \frac{d^2(r\Phi_{\text{III}}(r))}{dr^2} + \kappa_D^2 \Phi_{\text{III}}(r) = 0 \quad (27)$$

is satisfied by

$$\Phi_{\text{III}}(r \geq R + w) = B \frac{\exp(-\kappa_D r)}{r}. \quad (28)$$

Here the inverse square of the Debye screening length is given by $\kappa_D^2 = 2n_I \beta e_0^2 / \epsilon_w \epsilon_0$, where n_I is the bulk electrolyte ionic concentration.

Above we have obviously assumed that the two compartment (I and III) are in chemical equilibrium and can exchange electrolyte solution ions. If this is not the case, the screening properties, $\kappa_D(\text{I})$ and $\kappa_D(\text{III})$ would differ.

The electrostatic potentials in different regions are connected via boundary conditions that have the standard form

$$\epsilon_w \frac{\partial \Phi_{\text{I}}(r)}{\partial r} \Big|_{r=R} - \epsilon_p \frac{\partial \Phi_{\text{II}}(r)}{\partial r} \Big|_{r=R} = \frac{\sigma_1}{\epsilon_0}, \quad (29)$$

and

$$\epsilon_p \frac{\partial \Phi_{\text{II}}(r)}{\partial r} \Big|_{r=R+w} - \epsilon_w \frac{\partial \Phi_{\text{III}}(r)}{\partial r} \Big|_{r=R+w} = \frac{\sigma_2}{\epsilon_0}. \quad (30)$$

The four unknown coefficients, A, B, C , and D are obtained from the boundary conditions and have the form obtained previously in [55]

$$A = \mathcal{A}/\Delta, \quad B = \mathcal{B}/\Delta, \quad C = \mathcal{C}/\Delta, \quad D = \mathcal{D}/\Delta, \quad (31)$$

where

$$\begin{aligned} \Delta = & \epsilon_0 \epsilon_w \{ (\epsilon_p - \epsilon_w) \kappa_D w^2 + \epsilon_p \kappa_D R^2 \\ & + [\epsilon_p (1 + 2\kappa_D R) - \epsilon_w (1 + \kappa_D R)] w + \kappa_D R \\ & \times [\epsilon_w w^2 \kappa_D + \epsilon_p R + \epsilon_w (1 + \kappa_D R) w] \coth(\kappa_D R) \}, \end{aligned} \quad (32)$$

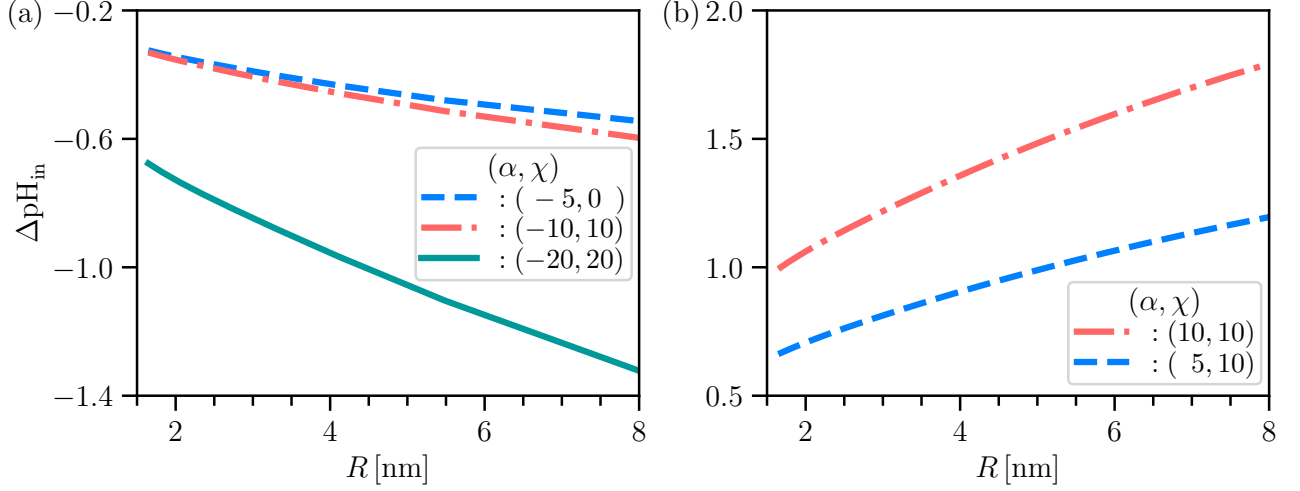


FIG. 11. Plot of $\Delta\text{pH}_{\text{in}}$ vs R . The inverse Debye length κ_D is fixed at 1.215 nm^{-1} . σ_1 and σ_2 are obtained from the CR process. The plots are shown for $\alpha < 0$ (a) and $\alpha > 0$ (b). $\Delta\text{pH}_{\text{in}}$ decreases (a)/increases (b) when the size of the vesicle increases.

and

$$\begin{aligned}
 \mathcal{A} &= \epsilon_w \sigma_1 R^2 \kappa_D w^2 + \epsilon_p [\sigma_1 R^2 + \sigma_2 (R+w)^2] R, \\
 &\quad + \epsilon_w \sigma_1 (1 + \kappa_D R) w R^2 \text{csch}(\kappa_D R) \\
 \mathcal{B} &= \{ [\epsilon_p \sigma_1 R^2 + \sigma_2 (R+w)^2] - \epsilon_w \sigma_2 (R+w)^2 \} w \\
 &\quad + \epsilon_p [\sigma_1 R^2 + \sigma_2 (R+w)^2] R \\
 &\quad + \epsilon_w \sigma_2 (R+w)^2 \delta \kappa_D R \coth(\kappa_D R) \exp[\kappa_D (R+w)], \\
 \mathcal{C} &= \epsilon_w \{ \sigma_1 w^2 \kappa_D R^2 + [\sigma_1 R^2 + \sigma_2 (R+w)^2] R \\
 &\quad + \sigma_1 R^2 (1 + 2\kappa_D R) w \\
 &\quad - \sigma_2 (R+w)^2 \kappa_D \coth(\kappa_D R) \}, \\
 \mathcal{D} &= \epsilon_p [\sigma_1 R^2 + \sigma_2 (R+w)^2] \\
 &\quad - \epsilon_w [\sigma_1 R^2 + \sigma_2 (R+w)^2 + \sigma_1 R^2 \kappa_D (R+w)] \\
 &\quad + \epsilon_w \kappa_D \sigma_2 (R+w)^2 R \coth(\kappa_D R). \tag{33}
 \end{aligned}$$

The results quoted in the main text are based on the various limits stemming from these expressions.

B. Comparison between the full Poisson-Boltzmann and the approximate Debye-Hückel solutions

Here we compare the linearized DH solution with the full numerical solution of the PB equation. Technically this refers to solutions of the full PB equation

$$\frac{1}{r} \frac{d^2(r\Phi(r))}{dr^2} + \frac{\kappa_D^2}{\beta e_0} \sinh \beta e_0 \Phi(r) = 0 \tag{34}$$

and the linearized DH equation

$$\frac{1}{r} \frac{d^2(r\Phi(r))}{dr^2} + \kappa_D^2 \Phi(r) = 0 \tag{35}$$

in the regions (I and III) accessible to the electrolyte ions. The methodology for obtaining the PB numerics has been

explained in details in our previous publications [20–22] and will not be elaborated here.

In Figs. 8 and 9 we compare the spatial profile of pH as obtained from the PB and the DH solutions. We notice that overall the difference for the chosen values of the parameters is small, but is smaller for $\alpha \leq 0$, Fig. 8, than for $\alpha \geq 0$, Fig. 9. In fact for large positive α the DH solution ceases to be a good approximation for the PB result, which would invalidate the DH approach. We also specifically indicate the difference in the surface charge densities $\Delta\sigma_i = \sigma_i^{\text{PB}} - \sigma_i^{\text{DH}}$ obtained from the two approaches in order to facilitate the comparison.

One conclusion following from the numerical results of the PB and DH approaches is that qualitatively they are very similar, but for certain values of the parameters there are quantitative differences. It seems that one can thus safely use the DH approximation if the focus is on the qualitative features, whereas a PB based calculation would be needed in order to do quantitative comparisons.

Concerning the quantitative mismatch between the PB and DH theories, we see the same trends as reported earlier [25]. For equal surface charge densities, linear DH theory overestimates the electrostatic potential. As our current study suggests, this remains true even when charge regulation is included unless the surface charge densities computed within the two theories do not vary too much. For significantly larger $\Delta\sigma_i$, as it is the case for the luminal region in Fig. 8(b), the electrostatic potential and the corresponding pH can of course be larger for the PB theory.

C. Curvature expansion parameters

In writing down the DH electrostatic free energy in the curvature expanded form Eq. 7 (see [24] for details), itself being based on the solution of the DH equation [55], we

introduced the following quantities

$$f_0(\sigma_1, \sigma_2, \kappa_D, w) = \frac{\mu(\sigma_1 + \sigma_2)^2 + \kappa_D w(\sigma_1^2 + \sigma_2^2)}{2\mu + \kappa_D w}, \quad (36)$$

$$f_1(\sigma_1, \sigma_2, \kappa_D, w) = \kappa_D w \left(\frac{(3\mu + 2(\kappa_D w) - 1)\sigma_2^2 + 2\mu\sigma_1\sigma_2 - (\mu - 1)\sigma_1^2}{2\mu + (\kappa_D w)} \right), \quad (37)$$

and

$$f_2(\sigma_1, \sigma_2, \kappa_D, w) = \frac{\kappa_D w}{(2\mu + (\kappa_D w))^2} \left((\mu - 1)[(\kappa_D w)(\mu - 1) - \mu]\sigma_1^2 - 2\mu((\kappa_D w) + 1)(\mu - 1)\sigma_1\sigma_2 + [(\kappa_D w)^3 + (\kappa_D w)^2(4\mu - 1) + (\kappa_D w)(5\mu^2 - 4\mu + 1) - \mu(\mu - 1)]\sigma_2^2 \right) \quad (38)$$

that do not depend on the curvature of the membrane anymore. In addition, for the curved membrane, f_0 , f_1 and f_2 are not symmetric with respect to the two solvent accessible inner and outer surface charge densities.

D. Dependence of $\Delta\text{pH}_{\text{m}}$, $\Delta\text{pH}_{\text{in}}$, $\Delta\text{pH}_{\text{out}}$ on curvature

Taking into account the DH solution for Φ_{I} , Φ_{II} and Φ_{III} above, and the definition of the constants $A = A(R, w)$, $B = B(R, w)$ and $C = C(R, w)$ in Eq. 33 that explicitly depend on R, w , we can rewrite the equations for the changes of the acidity Eqs. 16, 17 and 18 in the explicit form

$$\begin{aligned} \Delta\text{pH}_{\text{m}} &= \text{pH}(R + w) - \text{pH}(R) \\ &= \beta e_0 \log_{10} e \left(B(R, w) \frac{\exp(-\kappa_D(R + w))}{(R + w)} - A(R, w) \frac{\sinh(\kappa_D R)}{R} \right), \end{aligned} \quad (39)$$

$$\begin{aligned} \Delta\text{pH}_{\text{out}} &= \text{pH}(r = R + w) - \text{pH}^0 \\ &= \beta e_0 \log_{10} e B(R, w) \frac{\exp(-\kappa_D(R + w))}{R + w}, \end{aligned} \quad (40)$$

and

$$\begin{aligned} \Delta\text{pH}_{\text{in}} &= \text{pH}(r = R) - \text{pH}^0 \\ &= \beta e_0 \log_{10} e A(R, w) \frac{\sinh(\kappa_D R)}{R}. \end{aligned} \quad (41)$$

Figures 10 and 11 show the plots of $\Delta\text{pH}_{\text{in}}$ vs R with the rest of the parameters the same as before. Figure. 11 shows that $\Delta\text{pH}_{\text{in}}$ decreases when we increase the size of the vesicle for $\alpha < 0$ (Fig. 11(a)). While $\Delta\text{pH}_{\text{in}}$ increases when the size of the vesicle increases for $\alpha > 0$ (Fig. 11(b)). In addition, in Fig. 10, we found that the dependence of $\Delta\text{pH}_{\text{in}}$ on the radius, R , can be show increase, decrease or remain constant, depending on the values of the parameters (α, χ). What is particularly interesting is the "critical isotherm" corresponding to $\chi = -2\alpha$ case that shows no variation with radius up to a critical value and after that a non-monotonic dependence. Figure. 10 shows the case of $\chi = 0$ (no surface interaction). The plots are for both $\alpha < 0$ (Fig. 10(b)) and $\alpha > 0$ (Fig. 10(c)). We found that the $\Delta\text{pH}_{\text{in}}$ are the same but different in sign.

-
- [1] G. Cevc, in *Encyclopedia of Biophysics*, edited by G. C. K. Roberts and A. Watts (Springer Berlin Heidelberg, 2018) pp. 1446–1452.
[2] V. P. Zhdanov, *Eur. Biophys. J.* **52**, 121 (2023).
[3] K. Holmberg, B. Jönsson, B. Kronberg, and B. Lindman, *Surfactants and polymers in aqueous solution* (John Wiley & Sons, Ltd, 2002) pp. 1–525.

- [4] H.-X. Zhou and X. Pang, *Chem. Rev.* **118**, 1691 (2018).
[5] T. Simonson, *Rep. Prog. Phys.* **66**, 737 (2003).
[6] R. J. Nap, A. L. Božič, I. Szleifer, and R. Podgornik, *Biophys. J.* **107**, 1970 (2014).
[7] V. V. Galassi and N. Wilke, *Membranes* **11**, 478 (2021).
[8] P. Khunpetch, A. Majee, and R. Podgornik, *Soft Matter* **18**, 2597 (2022).

- [9] G. Cevc, *Biochimica et Biophysica Acta (BBA) - Reviews on Biomembranes* **1031**, 311 (1990).
- [10] V. Panagiotopoulou, *A theoretical and experimental study of cell membrane electrostatics and transport*, Ph.D. thesis, University of Nottingham (2012).
- [11] Y. Sarkar, R. Majumder, S. Das, A. Ray, and P. P. Parui, *Langmuir* **34**, 6271 (2018).
- [12] R. Zandi, B. Dragnea, A. Travesset, and R. Podgornik, *Phys. Rep.* **847**, 1 (2020).
- [13] L. Javidpour, A. Božič, A. Naji, and R. Podgornik, *Soft Matter* **17**, 4296 (2021).
- [14] D. Rochal, O. Konevtsova, A. Lošdorfer Božič, R. Podgornik, and S. Rochal, *Sci. Rep.* **9**, 5341 (2019).
- [15] O. V. Konevtsova, D. S. Roshal, A. Lošdorfer Božič, R. Podgornik, and S. Roshal, *Soft Matter* **15**, 7663 (2019).
- [16] S. B. Rochal, O. V. Konevtsova, D. S. Roshal, A. Božič, I. Y. Golushko, and R. Podgornik, *Nanoscale Adv.* **4**, 4677 (2022).
- [17] G. S. Longo, M. Olvera de la Cruz, and I. Szleifer, *Macromolecules* **44**, 147 (2011).
- [18] G. S. Longo, M. Olvera de la Cruz, and I. Szleifer, *ACS Nano* **7**, 2693 (2013).
- [19] M. I. Angelova, A.-F. Bitbol, M. Seigneuret, G. Staneva, A. Kodama, Y. Sakuma, T. Kawakatsu, M. Imai, and N. Puff, *Biochim. Biophys. Acta, Biomembr.* **1860**, 2042 (2018).
- [20] A. Majee, M. Bier, and R. Podgornik, *Soft Matter* **14**, 985 (2018).
- [21] A. Majee, M. Bier, R. Blossey, and R. Podgornik, *Phys. Rev. E* **100**, 050601 (2019).
- [22] A. Majee, M. Bier, R. Blossey, and R. Podgornik, *Phys. Rev. Research* **2**, 043417 (2020).
- [23] B. W. Ninham and V. A. Parsegian, *J. Theor. Biol.* **31**, 405 (1971).
- [24] H. R. Shojaei, A. L. Božič, M. Murugappan, and R. Podgornik, *Phys. Rev. E* **93**, 052415 (2016).
- [25] A. Majee, M. Bier, and S. Dietrich, *J. Chem. Phys.* **145**, 064707 (2016).
- [26] R. Bebon and A. Majee, *J. Chem. Phys.* **153**, 044903 (2020).
- [27] S. V. Siryk, A. Bendandi, A. Diaspro, and W. Rocchia, *J. Chem. Phys.* **155**, 114114 (2021).
- [28] S. V. Siryk and W. Rocchia, *J. Phys. Chem. B* **126**, 10400–10426 (2022).
- [29] T. Markovich, D. Andelman, and R. Podgornik, in *Handbook of Lipid Membranes*, edited by C. R. Safynia and J. O. Raedler (Taylor & Francis, 2021) pp. 99–128.
- [30] M. Muthukumar, *Physics of Charged Macromolecules. Synthetic and Biological Systems* (Cambridge University Press, 2023).
- [31] D. Andelman, in *Handbook of Biological Physics: Structure and Dynamics of Membranes*, edited by R. Lipowsky and E. Sackmann (Elsevier, 1995) pp. 603–642.
- [32] A. Fogden and B. Ninham, *Adv. Colloid Interface Sci.* **83**, 85 (1999).
- [33] E. J. Verwey and J. T. G. Overbeek, *Theory of the stability of Lyophobic Colloids* (Elsevier, Amsterdam, 1948).
- [34] M. Winterhalter and W. Helfrich, *J. Phys. Chem.* **92**, 6865 (1988).
- [35] D. J. Mitchell and B. W. Ninham, *Langmuir* **5**, 1121 (1989).
- [36] H. Lekkerkerker, *Physica A* **167**, 384 (1990).
- [37] B. Duplantier, R. E. Goldstein, V. Romero-Rochn, and A. I. Pesci, *Phys. Rev. Lett.* **65**, 508 (1990).
- [38] J. L. Harden, C. Marques, J. F. Joanny, and D. Andelman, *Langmuir* **8**, 1170 (1992).
- [39] L. Koopal, W. Tan, and M. Avena, *Adv. Colloid Interface Sci.* **280**, 102138 (2020).
- [40] M. Borkovec, B. Jönsson, and G. J. M. Koper, in *Surface and Colloid Science. Surface and Colloid Science*, edited by E. Matijević (2001) pp. 99–340.
- [41] Y. Avni, T. Markovich, R. Podgornik, and D. Andelman, *Soft Matter* **14**, 6058 (2018).
- [42] N. Adžić and R. Podgornik, *Eur. Phys. J. E* **37**, 49 (2014).
- [43] I. Teraoka, *Polymer solutions: An Introduction to Physical Properties* (John Wiley & Sons, Inc., New York, 2002).
- [44] Y. Avni, R. Podgornik, and D. Andelman, *J. Chem. Phys.* **153**, 024901 (2020).
- [45] R. Podgornik, *J. Chem. Phys.* **149**, 104701 (2018).
- [46] D. Harries, R. Podgornik, V. A. Parsegian, E. Mar-Or, and D. Andelman, *J. Chem. Phys.* **124**, 224702 (2006).
- [47] Y. Avni, D. Andelman, and R. Podgornik, *Curr. Opin. Electrochem.* **13**, 70 (2019).
- [48] S. L. Carnie and D. Y. Chan, *J. Colloid Interface Sci.* **161**, 260 (1993).
- [49] R. Pericet-Camara, G. Papastavrou, S. H. Behrens, and M. Borkovec, *J. Phys. Chem. B* **108**, 19467 (2004).
- [50] J. Landsgesell, L. Nová, O. Rud, F. Uhlík, D. Sean, P. Hebbeker, C. Holm, and P. Košovan, *Soft Matter* **15**, 1155 (2019).
- [51] J. Landsgesell, P. Hebbeker, O. Rud, R. Lunkad, P. Košovan, and C. Holm, *Macromolecules* **53**, 3007 (2020).
- [52] T. Chou, M. V. Jarić, and E. D. Siggia, *Biophys. J.* **72**, 2042 (1997).
- [53] R. Majumder, Y. Sarkar, S. Das, A. Ray, and P. P. Parui, *New J. Chem.* **41**, 8536 (2017).
- [54] H. J. Muhren and P. van der Schoot, *J. Phys. Chem. B* **127**, 2160 (2023).
- [55] A. Šiber and R. Podgornik, *Phys. Rev. E* **76**, 061906 (2007).